Estimation of Intramolecular Distance Distributions in Bovine Pancreatic Trypsin Inhibitor by Site-Specific Labeling and Nonradiative Excitation Energy-Transfer Measurements†

Dan Amir‡ and Elisha Haas*,‡,§

Department of Life Sciences, Bar-Ilan University, Ramat-Gan 52100, Israel, and Department of Biophysics and Chemical Physics, The Weizmann Institute of Science, Rehovot, Israel

Received April 16, 1986; Revised Manuscript Received December 8, 1986

ABSTRACT: A series of four bovine pancreatic trypsin inhibitor (BPTI) derivatives, site specifically labeled by (2-methoxy-1-naphthyl)methyl (MNA) at the N-terminal amino group and by [7-(dimethylamino)-coumarin-4-yl]acetyl (DA-coum) at one of the four ϵ-amino groups, was prepared. The four derivatives, N^{α}-MNA-Arg^{1}-N^{ϵ}-DA-coum-Lys^{n}-BPTI [(1-n)BPTI] (n = 15, 26, 41, and 46), were purified by affinity chromatography and high-performance liquid chromatography (HPLC). The homogeneity of each derivative and its site of labeling were characterized by HPLC tryptic peptide mapping. Nonradiative energy transfer from MNA (donor) to DA-coum (acceptor) was measured by monitoring donor emission and acceptor excitation spectra. Transfer efficiencies between 45% and 85% were observed. The fluorescence decay of MNA in MNA-BPTI, a derivative labeled by a donor without an acceptor, is monoexponential, with a lifetime of 6.8 ± 0.15 ns. The decay kinetics of MNA fluorescence measured for derivatives labeled both by donor and acceptor showed a small deviation from monoexponential decay with shorter average lifetimes. Analysis of the experimental decay curves yielded the detailed intramolecular distance distribution functions for each pair of labeled sites. The averages of the calculated distance distribution functions are close to the values expected from the known structure of BPTI in the crystalline state. The derivatives thus obtained are suitable for investigation of conformational transitions of the labeled protein and for monitoring localized changes such as those involved in the folding or unfolding transitions.

Globular proteins are characterized by well-defined ordered structures that determine their biological activity. A large number of structures of proteins in their crystalline state have been solved to a high resolution by the powerful methods of X-ray crystallography. The refined models built to fit the X-ray diffraction patterns gave insight to the mode of action and biological characteristics of many proteins. However, many aspects of protein function depend on their structural dynamics and multiplicity, which are presently not amenable to detailed analysis by existing X-ray methods. These include the following: (1) The possibility exists that the solution structures are different from that observed in the packed crystalline state. (2) Another aspect is protein folding, the transition of a denatured or nascent unordered polypeptide chain into an ordered native structure, which is a key process in the development of all organisms (Kim & Baldwin, 1982). Obviously, it should be studied by a method that can yield structural information about unordered structures. The same is true for the unfolding transition. (3) A third aspect is the dynamics of structures of globular proteins, which is the basis of many aspects of biology (Creighton, 1984a), including regulation (e.g., allosteric effect), activation, structural stability of protein molecules, and their ability to recover from transient environmental fluctuations. Only a few existing methods can yield directly interpretable structural details of the protein molecule in terms of intramolecular distances. Moreover, many conformational states appear to be a mixture of multiple conformations, e.g., denatured proteins or folding intermediates. This, in turn, leads to the regime of statistical approaches, searching for distributions of chain configurations and dynamics of segmental motions.

A few years ago we showed that measurements of nonradiative excitation energy transfer between donor and acceptor chromophores attached to a flexible polypeptide chain enabled us to determine the distribution of intramolecular distances between the labeled sites (Haas et al., 1975). It was also shown that intramolecular Brownian motions of the labeled segments can be measured down to the nanosecond time scale (Haas et al., 1978a). The results obtained with model polypeptides showed that the combination of site-specific labeling by chromophores with adequate spectral characteristics and fluorescence decay measurements should allow the development of a new experimental approach most suitable for studying protein structure in solution and its dynamic aspects mentioned above. This method has been under development in our laboratory for a number of years.

Bovine pancreatic trypsin inhibitor (BPTI),[1] a small and well-characterized protein (Creighton 1978), is used here as a model protein.

† Dedicated with appreciation and affection to Professor Ernest Fisher on the occasion of his 65th birthday. This study was supported by the U.S.-Israel Binational Science Foundation (Grants 2282/80 and 217/84). An EMBO fellowship to E.H. is gratefully acknowledged.

* Correspondence should be addressed to this author.

‡ Bar-Ilan University.

§ The Weizmann Institute of Science.

[1] Abbreviations: Bapa, *N*-benzoyl-DL-arginine-*p*-nitroanilide; bicine, *N,N*-bis(2-hydroxyethyl)glycine; BPTI, bovine pancreatic trypsin inhibitor; BTNA, *N*-benzoyl-DL-tyrosine-*p*-nitroanilide; DA-coum, [7-(dimethylamino)coumarin-4-yl]acetyl; DA-coum-BPTI, BPTI labeled by DA-coum at one of its amino groups; DMF, dimethylformamide; DTT, dithiothreitol; EDTA, ethylenediaminetetraacetate; Hepes, 4-(2-hydroxyethyl)-1-piperazineethanesulfonic acid; HPLC, high-performance liquid chromatography; Me_2SO, dimethyl sulfoxide; MNA, (2-methoxy-1-naphthyl)methyl; MNA-BPTI, BPTI labeled by MNA at the α-amino group of arginine-1; (1-n)BPTI, MNA-BPTI labeled by a DA-coum residue at one of its ϵ-amino groups; MNA-DA-coum-Lys or MD-Lys, N^{α}-MNA-N^{ϵ}-DA-coum-lysine or N^{α}-DA-coum-N^{ϵ}-MNA-lysine; NHSIE, *N*-hydroxysuccinimide ester; o.d., outer dimension; rf, radio frequency; TFA, trifluoroacetic acid; TPCK, L-1-(tosylamido)-2-phenylethyl chloroethyl ketone; Tris, tris(hydroxymethyl)aminomethane.

0006-2960/87/0426-2162$01.50/0

Procedures for the attachment of donor and acceptor probes to each one of the five amino groups of BPTI (four ϵ-amino groups of lysine side chains and the α-amino group of arginine-1 at the N-terminus) were developed (Amir & Haas, 1986a,b; Amir et al., 1986, 1985). Purification methods based on affinity chromatography and high-performance liquid chromatography (HPLC) were developed, as well as HPLC tryptic peptide mapping for determination of the labeled sites and specificity of the labeling procedures (Amir et al., 1985). In the following, we report a first step in the systematic study toward mapping the local segmental conformational states of BPTI by a combination of chemical modifications and nonradiative energy transfer measurements. Preliminary results were reported recently (Amir & Haas, 1986b). A series of four site specifically donor- and acceptor-labeled BPTI derivatives was prepared. The derivatives are active and can spontaneously refold after denaturation. Nonradiative energy transfer was measured both by steady-state methods and by fluorescence decay measurements for all the labeled derivatives. Four intramolecular distance distributions between the labeled sites were calculated for BPTI in its native state. The calculated distances between the N-terminal arginine residue and each one of the four lysine residues (residues 15, 26, 41, and 46) closely reproduce the distances expected from the coordinates of the labeled sites reported for the crystal structure of BPTI (Wlodawer et al., 1984).

The results presented herein demonstrate that our new approach should be instrumental in studying localized conformational transitions of globular proteins, e.g., the pathway of protein folding and regulatory transitions.

Theory

The probability $n_{D\to A}$ of energy transfer from a donor D to an acceptor A is given by (Förster, 1948)

$$n_{D\to A} = \frac{9000 \ln 10\kappa^2 Q}{128\pi^5 n^4 r^6 \tau} \int_0^\infty \frac{f(\bar{\nu})\epsilon(\bar{\nu})}{\bar{\nu}^4}\, d\bar{\nu} = \frac{1}{\tau}\left(\frac{R_0}{r}\right)^6 \quad (1)$$

where Q is the quantum yield of the donor in the absence of acceptor, n is the refractive index of the medium, N is Avogadro's number, r is the distance between the donor and the acceptor chromophores, τ is the lifetime of the donor in the absence of the acceptor, $f(\bar{\nu})\, d\bar{\nu}$ is the normalized fluorescence intensity of the donor in the wave number range $\bar{\nu}$ to $\bar{\nu} + d\bar{\nu}$, $\epsilon(\bar{\nu})$ is the molar absorption coefficient of the acceptor at wave number $\bar{\nu}$. κ^2 is a factor that expresses the orientational dependence of the probability of energy transfer. It has been shown (Haas et al., 1978b) that the orientational dependence of the probability of energy transfer can be made weak or insignificant by choosing donor and acceptor probes that exhibit low or medium limiting polarization characteristics for the electronic transitions involved in the transfer process. R_0, defined by eq 1, is given by

$$R_0^6 = (8.8 \times 10^{-25}) Q\kappa^2 n^{-4} J \ (\text{cm}^6) \quad (2)$$

J being the integral in eq 1. The energy-transfer process competes with all other processes for deexcitation of the donor characterized by the rate constant $1/\tau$.

For a population of labeled macromolecules in an unordered conformation, the interchromophoric distance is not unique; the efficiency of energy transfer from donor to acceptor measured for an ensemble of such molecules is thus an average quantity from which it is not possible to evaluate $f(r)$, the distribution function of intramolecular distances. It is, however, possible to reconstruct $f(r)$ by measuring the fluorescence decay kinetics of the donor instead of the efficiency of energy transfer (Haas et al., 1975). If the donor–acceptor distances are not changed during the lifetime of the excited state and all pairs of probes share the same value of R_0 (e.g., an isotropic or dynamic averaging of probe orientations), the donor fluorescence decays monoexponentially for each subpopulation of molecules, with a rate constant of $(1/\tau)[1 + (R_0/r)^6]$. The decay kinetics $I(t)$ for the total population of donor acceptor labeled molecules is thus given by

$$I(t) = k\int_0^{r_m} f(r) \exp\{-[t/\tau(1 + R_0^6/r^6)]\}\, dr \quad (3)$$

where k [which is $I(0)$] is proportional to the number of molecules and r_m is the distance of maximum separation between the donor and the acceptor. Obviously, $I(t)$ contains the information about $f(r)$, and methods were developed for estimation of $f(r)$ from the experimentally obtained fluorescence decay curve (Haas et al., 1975).

To evaluate the distribution function of the distances between donor and acceptor, one has to search for a function $f(r)$ which, when inserted in eq 3, gives an $I(t)$ that fits the experimental decay curves of the fluorescence of the donor. In the present study this search was done by using a model analytic distribution function with three free parameters. The parameters are adjusted by means of a least-squares procedure to give the best fit of a calculated decay curve, $I_c(t)$, computed from eq 3 and the experimental $I(t)$. The requirement is, of course, that $f(r)$ be flexible enough to accommodate the range of the real distribution functions of the protein studied.

The free parameters of $f(r)$ are changed by the least-squares algorithm to yield a best fit $F_c(t)$ (the theoretical system response to the fluorescence of the donor) and the experimentally measured fluorescence pulse $F(t)$. The criterion for best fit is minimalization of the root mean square deviation (RMS) between $F_c(t)$ and $F(t)$. Final judgment of the significance of the shape of the distribution function (in particular its average width and degree of skewness) is done by evaluation of the noise level and its randomness as estimated from the distribution of the deviations and their autocorrelation function (Grinvald & Steinberg, 1974).

In this study we have used for $f(r)$ an analytic expression of the form:

$$f(r) = c(4\pi)r^2 \exp[-a(r - b)^2] \quad (4)$$

where a and b are the adjustable parameters and c is the normalization constant. This expression was introduced by Edwards (1965) for the distribution of end-to-end distances of random coil polymers.

The two constants in eq 3, τ and R_0, are obtained from independent experiments. τ is obtained by measuring the fluorescence decay kinetics of the donor attached to a protein that is not labeled by an acceptor, under conditions identical with the conditions under which $F(t)$ is measured.

The value of R_0 is calculated according to the Förster theory (Förster, 1948) using eq 1 and 2. The overlap integral (J) and the donor fluorescence quantum yield (Q) are determined experimentally and contribute only a small uncertainty to the value of R_0 due to the sixth power relation in eq 2. Some degree of uncertainty is introduced by choice of the value of κ^2, the orientation factor, and n, the refractive index.

The index of refraction we have used in the calculation of R_0 is that of the solvent and not some higher value that might be estimated for the index of refraction of the interior of the protein. The space between the probes may be spanned by solvent or segments of the protein, depending on the sites labeled and the conformation. It is impossible to get a consensus estimation of the refractive index of the interior of a

protein (Warshel & Russel, 1984). Moreover, this being a property of a continuum, it is not simply justified to define a simple index of refraction for a structured microscopic space within a protein molecule and on its surface. We have followed the arguments presented by Moong et al. (1982) and used the index of refraction of the bulk solution in calculation of R_0.

Materials and Methods

Materials

Spectrograde cyclohexane was obtained from Fluka (Buchs). Glycogen (rabbit liver) was obtained from British Drug House (BDH, Poole), lot no. 1687970. Guanidine hydrochloride and urea (both Ultrapure) were obtained from Schwarz/Mann (Spring Valley, NY) and used as provided. Bovine pancreatic trypsin inhibitor (BPTI) Trasylol was a kind gift of Bayer, AG, Wuppertal (lot 1/79); Sephadex G-15 was a product of Pharmacia (Upsala). Sodium acetate (analytical grade) and trifluoroacetic acid (TFA) were products of Merck (Darmstadt). Tetrahydrofuran (THF) (Merck, Darmstadt) was distilled over $LiAlH_4$ prior to use. Methanol (Analar grade) and acetonitrile (HPLC grade) were used as supplied by Biolab (Jerusalem). All other solvents were of analytical grade. Dimethyl sulfoxide (Me_2SO) (distilled under vacuum prior to use) was obtained from Fluka (Buchs). Tris [lot 99C-01002 (base) and lot 56C-5042 (HCl)] and *N,N*-bis(2-hydroxyethyl)glycine (bicine) (lot 109C-5042) were purchased from Sigma (St. Louis). Analytical grade potassium chloride, calcium chloride, and glacial acetic acid were from Frutarom (Haifa). Trypsin (grade II), 4-(2-hydroxyethyl)-1-piperazineethanesulfonic acid (Hepes), *N*-benzoyl-DL-tyrosine-*p*-nitroanilide (BTNA), *N*-benzoyl-DL-arginine-*p*-nitroanilide (Bapa), DL-dithiothreitol (DTT), oxidized glutathione, ethylenediaminetetraacetic acid (EDTA), and L-lysine were obtained from Sigma. 7-(Dimethylamino)coumarin-4-acetic acid (DA-coum) was obtained from Molecular Probes (Junction City, OR). 2-Methoxy-1-naphthyl aldehyde (recrystallized from ethanol) and sodium cyanoborohydride were purchased from Aldrich (Milwaukee).

Methods

High-Performance Liquid Chromatography of Protein Derivatives. A Waters Associates (Milford, MA) HPLC system was used, which included the following nonstandard components: a Rheodyne (Cotati, CA) Model 7125 injector valve, Tracor (Austin, TX) Model 970A variable-wavelength spectrophotometer, and a Kratos Model FS 950 (Schoeffel Instruments, Westwood, NJ) flow fluorometer connected in tandem with the spectrophotometer. A Hewlett-Packard 3990A recording integrator and Yokogawa (Tokyo) type 3040 recorder were used for recording the UV and fluorescence signals, respectively. Fluorescence excitation wavelength 240–300 nm was selected by an interference filter. Emission wavelength was either 418 nm and above or 340 nm and higher selected by corresponding cutoff filters. Labeled protein preparations were fractionated by HPLC on a Nucleosil-10 RP-18 10-μm (Machery Nagel, Duren, FRG) columns (4.6 × 250 mm) in a gradient elution mode. The starting buffer, 0.1 M sodium acetate, pH 6.25 (buffer A), was modified by two linear gradients of increasing concentrations of THF: 0–7% in 2 min followed by 7–15% in 25 min. Special care was taken to use only freshly distilled THF (distilled over $LiAlH_4$) which was kept protected from light and under constant bubbling of argon or helium to prevent the formation of peroxides. The isolated fractions were collected and immediately subjected to evaporation of the organic solvent in a Speedvac concentrator centrifuge (Savant, Hicksville, NY) under vacuum. Each derivative was rechromatographed by using the same chromatographic procedure.

Chromatography of Tryptic Peptides. Reduction, carboxymethylation, and tryptic digestion of BPTI and its derivatives were performed as described earlier (Amir & Haas, 1986a). The peptide mapping was done on a 10-μm reverse-phase C_8 radial PAK cartridge (Waters Associates). Separation [except for (1-15)BPTI] was achieved by the use of a biphasic linear gradient from 0.05 M sodium phosphate at pH 3.5 (solvent A) to 65% acetonitrile in solvent A (solvent B) at a constant rate of 1.5 mL min^{-1}. The columnn was equilibrated with solvent A and then eluted by a linear gradient of 0–20% acetonitrile in 10 min followed by a second phase increasing acetonitrile content from 20% to 65% in 25 min.

For peptide mapping of (1-15)BPTI, a 10-μm reverse-phase C_{18} radial PAK cartridge (Waters Associates) was used. Solvents A and B were the same, and a linear gradient of 0–20% acetonitrile in 10 min was used, followed by a second phase increasing acetonitrile content from 20% to 40% in 25 min and from 40% to 75% acetonitrile in 5 min.

Solvents were degassed by a constant slow flow of helium. All runs were performed at room temperature.

Affinity Chromatography of Labeled BPTI. Affinity chromatography of labeled BPTI was a modification of the procedure described earlier (Amir & Haas, 1986a). A trypsin–Sepharose column (1 × 20 cm) was equilibrated with 0.1 M bicine buffer, pH 8.0, containing 50 mM $CaCl_2$ at a flow rate of 1.0 mL/min. Two protein fractions were eluted in two pH steps: first, with 0.05 M sodium acetate buffer, pH 3.5, followed by a second step with 2 M guanidine hydrochloride in 0.1 M acetic acid, pH 2.5. The second fraction which contained guanidine hydrochloride, was neutralized with concentrated sodium hydroxide, diluted by an equal volume of 0.1 M bicine buffer, pH 8.0, containing 50 mM $CaCl_2$, and applied to a chymotrypsin–Sepharose 4B column (1 × 20 cm). The column was washed by distilled water, and the desalted BPTI was eluted as a single narrow peak by 0.1 M acetic acid, pH 2.5. The elution profile of each column was recorded by an LKB (Broma) UV monitor.

Assay of Enzymatic Activity. Trypsin was routinely assayed by its hydrolysis of N^{α}-benzoyl-DL-arginine-*p*-nitroanilide (Bapa) by the method of Erlanger et al. (1961). Chymotrypsin was assayed by its hydrolysis of *N*-benzoyl-L-tyrosine-*p*-nitroanilide (BTNA) by the method of Bundy (1962). The inhibitor was assayed by its stoichiometric inhibition of trypsin, as described by Kassel (1970).

Denaturation and Renaturation of BPTI Derivatives. BPTI derivatives (18 μM) were reduced in 0.1 M bicine buffer at pH 8.0, 6 M guanidine hydrochloride, 1 mM EDTA, and 10 mM DTT for 10 h at room temperature. The protein samples were diluted 12-fold with 0.1 M bicine buffer at pH 8.0, 1 mM EDTA, and 1.1 mM oxidized glutathione at room temperature. After 3 h, the trypsin inhibitor activity of each sample was tested and compared to that of untreated derivative.

Amino acid analyses were carried out on a Dionex (Model D502) analyzer equipped with an Aminex column.

Steady-State Fluorescence Measurements. Fluorescence spectra were recorded on a Perkin-Elmer (Norwalk, CT) Model MPF-44 spectrofluorometer. The absorbance of the samples at 380 nm was in the range of 0.05–0.15. The sample solution was placed in a quartz cell made from a square cross section quartz tube obtained from Hareus Quartzschmelze (Hanau, FRG) (3 × 3 mm internal cross section, 5 × 5 mm o.d.). For low-temperature measurements a quartz Dewar

made by Helma (Muellheim/Baden, FRG) was used (o.d. 34 mm, i.d. 24 mm, height 115 mm). A copper block (diameter 23.2 mm, height 80 mm) was used as a cell holder fitted in the quartz Dewar. The block was cooled by cold nitrogen pumped from a liquid nitrogen container. The flow of the cold nitrogen was controlled by a Wellco temperature controller (Barber-Colman type J).

Fluorescence Lifetime Measurements. Fluorescence lifetime measurements were made by using an instrument based on the pulse sampling technique, as described previously (Handley et al., 1967; Hazan, 1973; Hazan et al., 1974). A deuterium flash lamp (TRW Inc., Torrance, CA) was used as an excitation source with a homemade high-voltage power supply enclosed in a brass housing which reduces the rf noise. The excitation wavelength was selected by a combination of two filters, viz., a 1-cm path length chemical filter containing a mixture of K_2CrO_4 (0.270 g/L) and Na_2CO_3 (1.0 g/L) in water and a Schott (Mainz, FRG) UG11 glass absorbance filter. This combination has a transmission maximum at 315 nm, which overlaps a shoulder of the longest wavelength absorption band of MNA. The glass filter absorbs the visible light transmitted by the chemical filter. In some experiments, an interference filter with a 10-nm band-pass and transmission at 332.5 nm (Schott, Mainz, FRG) was used.

The emitted light was detected at 90° by an XP1023 photomultiplier tube (Phillips, Eindnoven, The Netherlands) and at a wavelength selected by a combination of two glass filters, Kodak 18A and Schott (Mainz, FRG) WG360 cutoff filter. This combination transmits a broad band in the wavelength range 350–380 nm and thus selects for MNA fluorescence and rejects most of the scattered light and all of the acceptor's emission.

The averaged excitation and emission pulse profile data were transferred to an IBM 3801 computer by means of an Apple-type microcomputer. Corrections due to Rayleigh and Raman scattering and due to the background fluorescence were made as described previously (Haas et al., 1978a). Time calibration of the system was made by a pretrigger pulse generator (type 111, Tektronix, Inc., Portland, OR) equipped with either 9- or 20-ns charge lines. The system was tested routinely for calibration and linearity by measurements of the fluorescence decay constant of a cyclohexane solution of zone-refined anthracene (kindly provided by Dr. Z. Ludmir); this material gives a monoexponential decay with a lifetime of 4.0 ± 0.08 ns for undegassed solutions [compared to a value of 4.9 ns for a degassed solution (Berlman, 1965)].

Results

Preparation of Site-Specific Donor–Acceptor-Labeled BPTI Derivatives. Recently, we have reported two procedures for the preparation of site specifically labeled fluorescent BPTI derivatives (Amir et al., 1986; Amir & Haas, 1986a). Both procedures are based on nonselective alkylation or acylation reactions without protection, generating a mixture of products that is resolved by affinity chromatography and HPLC. We have used both procedures in order to prepare doubly labeled BPTI derivatives, each containing a single donor chromophore (MNA) at the N-terminal amino group and a single acceptor (DA-coum) chromophore at a well-defined site on one of the ϵ-amino groups of BPTI.

N^{α}-MNA-Arg^1-BPTI (MNA-BPTI) was prepared by reductive alkylation, purified (Amir et al., 1986), and then labeled by a second probe (an acceptor) by a limited nonselective acylation reaction. The HPLC-purified MNA-BPTI was desalted on an α-chymotrypsin–Sepharose affinity column, and the neutralized aqueous fractions were concentrated in a Speedvac concentrator. Freshly distilled Me_2SO was added, and the evaporation in the Speedvac concentrator was continued until dry Me_2SO solution of the protein was obtained. Acylation by succinimido 7-(dimethylamino)coumarin-4-acetate (DA-NHSIE) was carried out for a limited time.

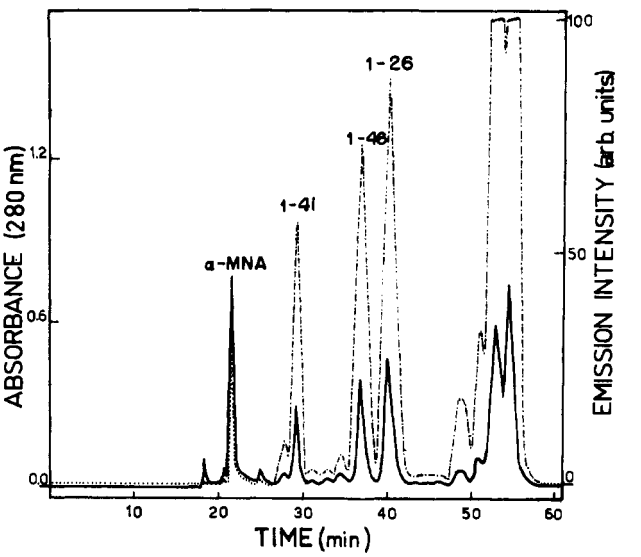

FIGURE 1: Reverse-phase HPLC separation of donor–acceptor-labeled BPTI. MNA-BPTI was nonselectively labeled by DA-coum-NHSIE, and the mixture was fractionated on 10-μm C_{18} Nucleosil-10 reversed-phase column. A gradient of THF in 0.1 M NaOAc was used. The column was monitored by a UV spectrophotometer (—) and a fluorometer (excitation wavelength 240–300 nm, emission wavelength >320 nm). The first fraction (MNA-BPTI) had only UV fluorescence (···); the others had both UV and visible emissions [peaking at 360 and 480 nm (–·–)]. The first four fractions were identified by tryptic mapping, and the labeled sites are indicated. The last fractions were triply labeled (one MNA and two or more DA-coum chromophores).

The reaction mixture was fractionated on a trypsin–Sepharose column, essentially as described earlier (Amir & Haas, 1986a). The product mixture of the high-affinity fraction was desalted on a chymotrypsin–Sepharose column, and the two protein fractions were further resolved on a reverse-phase HPLC.

The HPLC separation of the high-affinity fraction eluted from the trypsin–Sepharose at low pH is shown in Figure 1. The first fraction (22 min, which had only MNA fluorescence (emission at 360 nm), was the unreacted MNA-BPTI. The second, third, and fourth fractions had both MNA and DA-coum fluorescence. Those three base line separated fractions are characterized by a closely similar ratio of DA-coum fluorescence and UV absorbance: 3.3 (arbitrary units). All three have the same ratio of DA-coum absorbance at 386 nm and the combined absorbance at 280 nm. On the basis of these observations alone, one can already deduce that these three products are isomeric single-donor single-acceptor labeled derivatives. Direct inspection of the chromatogram shows that the last fractions, eluted at 48 min and later, are multiply labeled BPTI derivatives containing a single MNA and two or more DA-coum chromophores. This is obvious from the ratio of the fluorescence emission (above 418 nm) and the absorbance at 280 nm, compared to that ratio observed for the monolabeled fractions. The first three doubly labeled fractions (marked 1–41, 1–46, and 1–26 in Figure 1) were rechromatographed under the same conditions on HPLC for improved purity. Each chromatogram was monitored by a UV spectrophotometer and by a filter fluorometer set for detection of the DA-coum fluorescence (emission cutoff filter transmitting above 418 nm, MNA fluorescence not transmitted). The excitation wavelength of the fluorescence monitor was 280

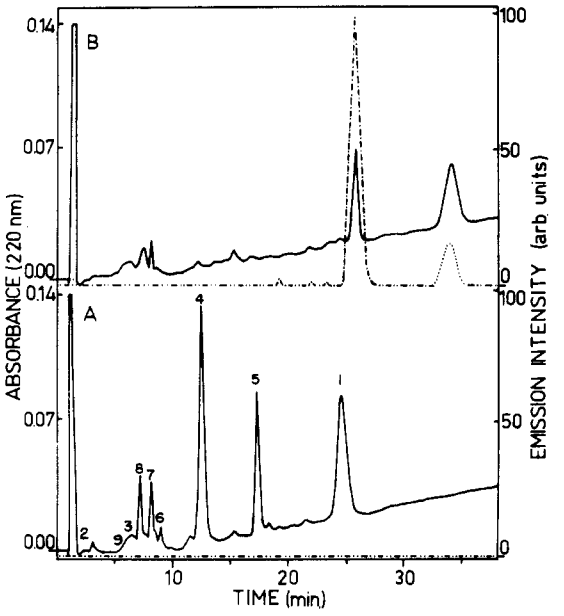

FIGURE 2: HPLC peptide map of the fourth fraction (1-26)BPTI separated from the second labeling cycle. The peptide mixture of tryptic digestion of carboxymethylated sample of the labeled protein (3 nmol) was eluted by a gradient of acetonitrile in 0.05 M phosphate buffer, pH 3.0. The eluant was monitored by a UV spectrometer at 220 nm and a fluorometer that monitors both donor and acceptor emission. (A) Peptide map of unlabeled, native BPTI; each peptide is marked by its position in the amino acid sequence. (B) Peptide map of the labeled sample. Note that three peptides are missing and two new fluorescent fractions are present.

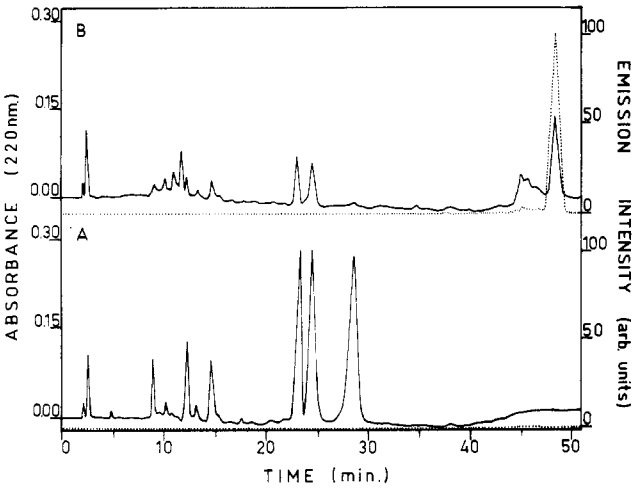

FIGURE 3: HPLC peptide map of low-affinity fraction, prepared as described in Figure 2. (A) Peptide map of unlabeled BPTI. (B) Peptide map of the labeled sample. Note that only one peptide (peptide 1, the N-terminus) was labeled by both probes; hence this derivative is labeled at residues 1 and 15.

nm, a wavelength at which the donor, MNA, absorbs more than the acceptor. Therefore, the concentration dependence of the fluorescence intensity of the labeled fractions in the chromatogram is not uniform, and the ratio of fluorescence intensity to absorbance is variable, depending on the transfer efficiency of each fraction.

The single site labeled by DA-coum in each derivative and the extent of purity of the products were determined by HPLC tryptic peptide mapping. Samples of the pure donor–acceptor-labeled derivatives were denatured, reduced, carboxymethylated, and digested by TPCK–trypsin. The resulting tryptic fragment mixtures were resolved on a reverse-phase HPLC column (Amir et al., 1985). Two examples of these

Table I: Amino Acid Composition of Fluorescent Peptides in Tryptic Peptide Maps of (1-*n*)BPTI Derivatives[a]

	peptide analyzed				
	UV fluorescent peptide of	amino acid composition of blue fluorescent peptides in[c]			
amino acid	MNA-BPTI[b]	1-41	1-46	1-26	1-15
Asp/Asn	1.0 (1)		3.1 (3)	1.0 (1)	0.9 (1)
Thr	1.0 (1)			0.8 (1)	1.0 (1)
Ser			1.2 (1)		
Glu/Gln	1.2 (1)		1.1 (1)	1.0 (1)	1.4 (1)
Pro	4.0 (4)				3.5 (4)
Gly	1.0 (1)			3.1 (3)	1.4 (1)
Val				0.8 (1)	
Ala		1.1 (1)	1.0 (1)	2.0 (2)	1.1 (1)
Cys	0.7 (2)		0.7 (1)	1.1 (2)	1.0 (2)
Met			0.6 (1)		
Leu	1.0 (1)			1.0 (1)	1.1 (1)
Tyr[d]	0.5 (1)			1.0 (3)	0.3 (1)
Phe[d]	0.9 (1)		0.9 (1)	1.0 (2)	0.8 (1)
Lys	0.9 (1)	1.0 (1)	1.1 (1)	0.9 (1)	1.0 (1)
Arg	0.9 (1)	1.0 (1)	1.0 (1)	1.1 (1)	1.5 (2)

[a] Samples (3–6 nmol) of each one of the doubly labeled (donor and acceptor) derivatives of BPTI separated as shown in Figure 1 were denatured, reduced, carboxymethylated, digested by TPCK–trypsin, and fractionated by HPLC as shown in Figures 2 and 3. The fluorescent peptides were analyzed, and the composition is shown for each derivative. [b] In each peptide map this same peptide was eluted at the same time, except for the case of (1-15)BPTI shown in Figure 2. [c] The first three are the corresponding fractions in Figure 1; 1-15 represents (1-15)BPTI. [d] The low recoveries of these amino acids are due to the absence of phenol in the hydrolysis solution.

tryptic peptide maps are shown in Figures 2 and 3. Nine peptides are found in the peptide map of unlabeled BPTI, and each fragment is marked in Figure 2A by its sequential position in the polypeptide. The chromatogram was monitored by the fluorometer using a filter combination that transmits both MNA and DA-coum emission. No fluorescence was detected when a nonlabeled BPTI was analyzed (Figure 2A). The peptide map of the DA-coum-labeled derivative eluted from the HPLC column as the fourth fraction, as shown in Figure 1, is shown in Figure 2B. Peptides 4, 5, and 1 are missing, and two new fluorescent fractions are found. The first, eluted at ca. 26 min, had a strong fluorescence intensity traced by the in-line fluorometer and identified later in a spectrofluorometer as a purely DA-coum emission. The second fluorescent fragment had a smaller intensity detected by the in-line fluorometer and identified as a pure MNA fluorescence. This last fragment is the N-terminal peptide (1) (residues 1–15) since it includes the MNA label shown earlier to be attached to Arg-1 (Amir et al., 1986a). The first fluorescent fragment appears to include both peptide 4 and peptide 5 and, hence, is labeled at Lys-26. (The differences in the fluorescence intensity observed for the two peptides are due to the higher sensitivity of the fluorometer at 480 nm and the higher quantum efficiency of DA-coum relative to that of MNA). This assignment is confirmed by the composition of the fluorescent fragments obtained from amino acid analysis (Table I). Hence, the peptide mapping shows that only Lys-26 was labeled in the second labeling step and that no more than 1% of BPTI labeled by MNA only may be found in this preparation.

Figure 3 shows the chromatogram of the tryptic peptide map of (1-15)BPTI. Only one fluorescent peptide was found, and only peptide 1 (see Figure 2A) was absent. Hence, the fluorescent fragment, which included both donor and acceptor fluorescence, was clearly the N-temrinal segment, and the tentative labeling assignment of (1-15)BPTI based on the affinity chromatography and HPLC was thus confirmed.

(Further confirmation of this assignment is obtained by amino acid analysis of the labeled peptide, Table I.)

In a similar procedure, the other two DA-coum-labeled fractions shown in Figure 1 were identified as (1-41)BPTI and (1-46)BPTI. The assignments based on the peptide mapping are indicated in Figure 1.

(1-15)BPTI was also prepared by using the same procedures described above, but in the reversed order. BPTI was labeled by DA-coum by using the *N*-hydroxysuccinimide ester in Me_2SO, as described earlier (Amir & Haas, 1986a). N^{ϵ}-DA-coum-Lys[15]-BPTI, isolated by affinity column and HPLC, was purified and then reductively alkylated by MNA. The main product, (1-15)BPTI, was obtained in a pure state from reverse-phase HPLC. Starting with 13.9 mg of MNA-BPTI, we obtained an overall yield of 4.85 mg of labeled protein. This was distributed to give 2.4 mg of unreacted MNA-BPTI (50%), 0.43 mg of (1-15)BPTI (9%), 0.62 mg of (1-26)BPTI (13%), 0.35 mg of (1-41)BPTI (7%), 0.45 mg of (1-46)BPTI (9%), and 0.6 mg of multiply DA-coum labeled MNA-BPTI.

The preparative and analytical procedures described in this section yielded a series of four pure BPTI derivatives, (1-*n*)-BPTI (*n* = 15, 26, 41, 46), each labeled by a single donor probe, MNA, at the N-terminal residue and by a single acceptor probe, DA-coum, at one of its four lysine residues. Each derivative has been unequivocally analyzed and assigned, and hence, we can approach the experiments of intramolecular distance determinations by energy-transfer measurements.

Characterization of Labeled Products. The fitness of the labeled products described above for conformational studies of BPTI by spectroscopic measurements depends on independent evaluation of the effect of the labels on the protein conformation. Measurements of enzymatic (or, when applicable, inhibitory) activity are a sensitive method for detecting conformational perturbations. All the labeled derivatives were found to be active as inhibitors of trypsin and chymotrypsin. Even the affinity chromatography step used in each preparation indicates that the same conditions were needed in order to release the labeled products from the trypsin–Sepharose and chymotrypsin–Sepharose columns.

The stoichiometric inhibition capacity of the derivatives not labeled at Lys-15 could not be distinguished from that of the unmodified protein. This shows that no major conformational alteration has taken place in those derivatives. It does not exclude possible minor conformational transitions, since, as has been noted earlier, the binding constant of BPTI and trypsin is very high ($K_d = 6 \times 10^{-14}$ M^{-1}) (Vincent & Lazdunski, 1972) so that even a factor of 10^{-3} reduction in the binding constant has an insignificant effect on the stoichiometric inhibition capacity of BPTI. The derivative labeled at Lys-15, the active site residue, shows reduced inhibitory activity as has been reported by many investigators who used other blocking groups (Vincent et al., 1974; Rigbi, 1970). This reduced activity is attributed to direct steric and charge effects of interference at the enzyme active site rather than conformational perturbations.

Samples of all the derivatives, except for the derivative blocked at lysine-15, were reduced by DTT in 6 M guanidine hydrochloride(Gdn-HCl) for 5 h, causing denaturation and complete loss of inhibitory activity. Dilution into refolding conditions [0.5 M Gdn-HCl, with an oxidizing agent (e.g., oxidized glutathione)] resulted in refolding and regain of the inhibitory activity. The kinetics of unfolding of all three derivatives at low concentration of BPTI, in the absence of Gdn-HCl, is 3-fold faster than that of native BPTI (with minor differences between them). Thus, blocking the amino groups of BPTI did not cause a gross conformational change in the protein and did not change its capacity to refold after denaturation. This is a strong indication that the derivatives prepared as described above are suitable for conformational studies of BPTI.

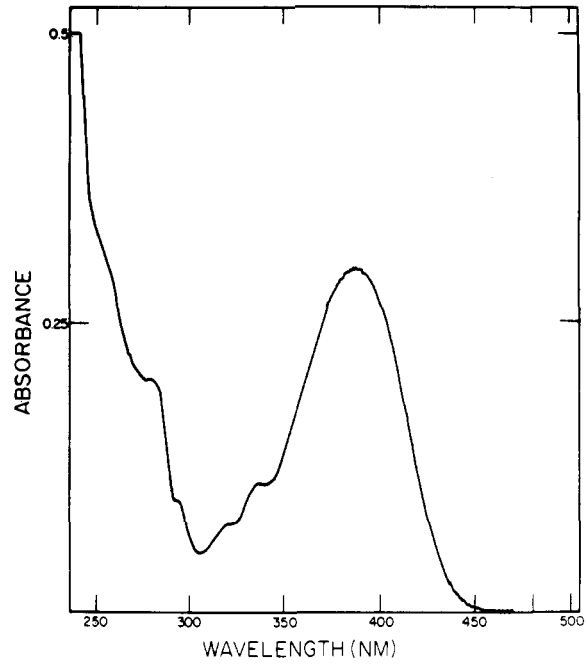

FIGURE 4: Absorption spectrum of donor- and acceptor-labeled BPTI [(1-26)BPTI]. The superposition of three components is visible, the protein's band at 280 nm, the donor's bands at 295, 323, and 338 nm, and the acceptor's band at 382 nm.

Spectral Characterization. The absorption spectra of BPTI labeled by a donor or by an acceptor were reported earlier (Amir et al., 1986; Amir & Haas, 1986a). Figure 4 shows the absorption spectrum of (1-26)BPTI (in aqueous buffer at neutral pH). As expected, this spectrum is a linear combination of three contributions corresponding to a ratio of protein:MNA:DA-coum of 1:1:1. The absorption bands at 295, 323 and 338 nm are characteristic of the MNA chromophore. These are superimposed on the absorption of the protein (at 276 nm, which overlaps the 285-nm band of MNA absorption) and the DA-coum absorption, which has a strong band at 382 nm [with extinction coefficients, at 280 nm, as follows: native BPTI, $\epsilon = 5250$; MNA, $\epsilon = 4400$ (amir et al., 1986); DA-coum, $\epsilon = 4000$ (Amir & Haas, 1986a)]. The four derivatives (1-*n*)BPTI (*n* = 15, 26, 41, 46) had identical absorption spectra; no relative spectral shifts were caused by the various sites to which the DA-coum was attached.

Value of R_0. Some of the variables that affect the magnitude of R_0 depend on the solution conditions (i.e., pH, Gdn-HCl concentration, temperature, etc.). For this reason, R_0 was calculated for each solution state studied, by making separate determinations of the quantum yield, Q, and the refractive index, n (eq 2). Figure 5 demonstrates some of the spectral characteristics of the probes relevant to the determination of R_0 and the measurement of transfer efficiency in labeled BPTI. The emission band of MNA at 360 nm is well resolved from the acceptor (DA-coum) emission centered at 482 nm. Thus, it is possible to resolve both emissions in the doubly labeled protein. The absorption of DA-coum-BPTI (with a maximum at 382 nm) strongly overlaps the emission of MNA.

The fluorescence quantum yield of MNA-BPTI was determined and found to be 0.2 ± 0.02 (Amir et al., 1986), in aqueous neutral solution. An average value of $^2/_3$ was assumed

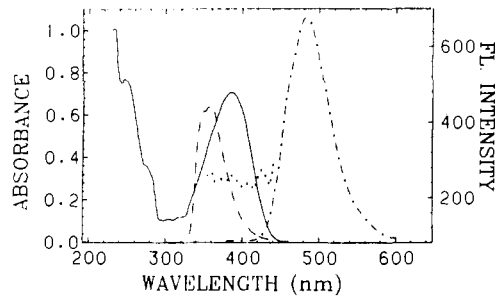

FIGURE 5: Spectral characteristics of the donor–acceptor pair of chromophores used for labeling BPTI. (---) Emission spectrum of MNA (centered at 360 nm) overlaps the absorption spectrum of DA-coum (recorded for N^{ϵ}-DA-coum-Lys^{26}-BPTI) (—). Emission of DA-coum (centered at cf. 480 nm) was recorded for the same derivatives by using excitation at 386 nm (–·–) (emission bandwidth 2 nm) and corrected by using quinine sulfate in 1 N H_2SO_4 as a reference. Excitation polarization spectrum of the DA-coum fluorescence is shown (···).

for the orientational factor, κ^2 (Haas et al., 1978b; see Discussion), and the refractive index of water was used as well. Using the above parameters and the spectral overlap integral (data presented in Figure 5 and eq 4), one obtains that R_0 for MNA-DA-coum pair in aqueous neutral solvents is 32.4 ± 2 Å.

Intramolecular Distance Determination in Native BPTI by Energy-Transfer Measurements. Steady-State Measurements. The fluorescence emission spectra of (1-*n*)BPTI (*n* = 15, 26, 41, 46) derivatives are shown in Figure 6. As expected from the spectral data of the monolabeled derivatives shown in Figure 5, two well-resolved emission bands are observed. The emission at 360 nm is contributed by the donor, MNA, and the second emission band peaking at 482 nm is the emission of the acceptor. The four derivatives differ markedly in their emission spectra, indicating differences in intramolecular distances. The ratio of the two emission bands qualitatively indicates that the distance between residues 1 and 15 (curve D) is the largest one measured in this series, while the distances from residue 1 to residues 46, 26, and 41 are considerably shorter, the last one being the shortest. This is in good agreement with the known interresidue distances calculated from X-ray crystallographic data (Wlodawer et al., 1984).

Two additional spectra are shown in Figure 6. The lowest curve (broken line) is the emission spectrum of BPTI labeled by the acceptor, without a donor, in which DA-coum was attached to the amino group of lysine-41. No emission is observed at the 360-nm band. The spectrum marked S is the emission spectrum of MNA-DA-coum-Lys (see below).

A Quantitative Estimation of Average Transfer Efficiencies Is Obtained from Acceptor Excitation Spectra. We have selected for this study a pair of probes that is characterized by well-resolved emission bands, and hence, one can follow the emission of the acceptor in a spectral range in which donor emission is negligible (>440 nm; see Figure 5). The large Stokes shift of the acceptor emission allows direct determination of transfer efficiencies from acceptor excitation spectra. It should be noted that, in this mode of transfer efficiency measurements, one relies on the analysis of the shape of the spectrum alone without additional input such as the concentration or absorbances required for analysis of transfer efficiencies from donor emission spectra. Thus, the shape of the excitation spectrum is an instrinsic property of the system dependent on variation of transfer efficiency only. This is so since all measurements are made under the same setting of the emission monochromator; no wavelength-dependent variation in the detector sensitivity can affect the results, and

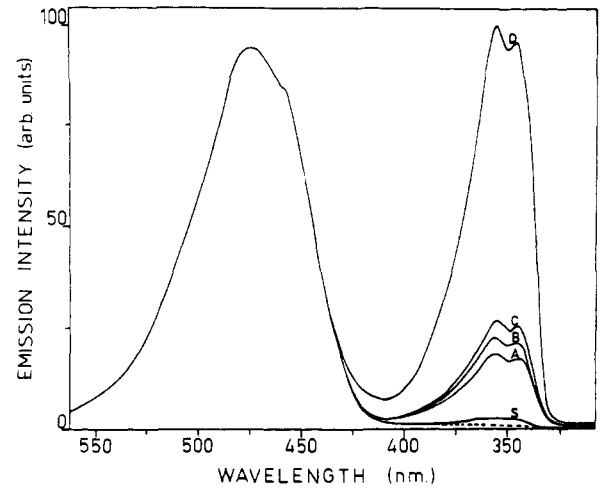

FIGURE 6: Fluorescence emission spectra (uncorrected) of labeled BPTI derivatives and reference compounds. Fluorescence emission of N^{ϵ}-DA-coum-Lys^{41}-BPTI (---), a derivative labeled by the acceptor only. Curves A–D are the fluorescence emission of BPTI derivatives labeled by a donor at the N-terminal amino group and an acceptor at ϵ-amino groups of lysine residues 41, 26, 46, and 15, respectively. Excitation wavelength 295 nm, excitation bandwidth 12 nm, emission bandwidth 2 nm. All spectra were recorded at room temperature and normalized to the same emission intensities at 480 nm. The emission at 360 nm is the donor fluorescence; it is considerably higher for (1-15)BPTI which has a larger interchromophoric distance and, hence, lower transfer efficiency. The trace marked S shows the emission of MNA-DA-coum-Lys, a low molecular weight reference compound with 97 ± 2% transfer efficiency, recorded under the above same conditions.

quenching effects also do not affect the spectrum unless affecting the transfer efficiency as in the case of quenching of donor emission, thus changing R_0. Quantitative analysis of excitation spectra is simpler when spectra are compared to those of a derivative characterized by zero transfer efficiency and a derivative known to have a constant high transfer efficiency. The first derivative is readily available; any DA-coum-BPTI derivative supplies the "base line" of direct acceptor excitation in the spectral range of donor absorption. As shown in Figure 5, the pair of probes used here are ideal from this point of view since in the range of 290–340 nm, which is between the main absorption bands of the protein and those of the acceptor, the acceptor absorption is relatively low, with a "window" free for detection of donor excitation. The second derivative was prepared by attaching both probes to the two amino groups of lysine acid. Two pure MNA-DA-coum-Lys isomers were prepared, which show a 1:1 ratio of MNA to DA-coum absorption. No indication of a modified absorption spectrum could be detected. The absorption and acceptor excitation spectra of the two isomers of MNA-DA-coum-Lys are very similar, which is a qualitative indication of high transfer efficiency. Both absorption by the donor and that by the acceptor contribute to the acceptor emission. Furthermore, curve S in Figure 6 shows that only very low intensity of emission is monitored in the donor emission spectral band for this compound. Fluorescence decay measurements show that this residual emission is characterized by a lifetime of 0.2 ns. Thus, it is concluded that it is not a contribution of a contamination of lysine labeled by a donor without an acceptor and that transfer efficiency in this reference compound is 97 ± 2%. The second derivative isolated by HPLC was found to have a very close transfer efficiency by the same criterion. These two derivatives are probably two permutations of the labeling sites by the donor and acceptor; however, since a rigorous identification of their structures is irrelevant to the present study, further analysis of the structure of these de-

Table II: Transfer Efficiencies and Intramolecular Distances Measured for (1-*n*)BPTI in the Native State

derivatives	E^a	E^b	R (Å)^c	R_x (Å)^d	W (Å)^e	ϕ (ns)^f MNA	ϕ (ns)^g
1-15	0.45 ± 0.05	0.44 ± 0.05	34 ± 1	31.7	9 ± 1.5	1.2 ± 0.1	0.48 ± 0.05
1-26	0.79 ± 0.05	0.84 ± 0.05	22 ± 1	16.8	9 ± 1.5	1.0 ± 0.1	0.46 ± 0.05
1-41	0.85 ± 0.05	0.85 ± 0.05	21 ± 1	18.0	11 ± 1.5	0.9 ± 0.1	0.58 ± 0.05
1-46	0.78 ± 0.05	0.80 ± 0.05	23 ± 1.5	21.7	10 ± 1.5	0.6 ± 0.2	0.45 ± 0.05
MNA-BPTI						1.2 ± 0.1	
DA-coum-BPTI							0.5 ± 0.05

[a] Transfer efficiency calculated from excitation spectra. [b] Transfer efficiency estimated from multiexponential analysis of donor fluorescence decay curves. [c] Square root of the second moment of the distance distribution functions. [d] Distance between the two labeled amino groups calculated from atomic coordinates reported for the crystal structure (Wlodawer et al., 1984). [e] Width at half-height of the distance distribution functions. [f] Average correlation time calculated from depolarization measurements and average lifetime data presented in Table III by using the Perrin equation. [g] Average rotational correlation time calculated for the acceptor, DA-coum.

rivatives is deferred to a later time.

An essential control should be done in order to make sure that, in the concentration range of dilute solutions of BPTI used in the present study, no intermolecular excitation energy transfer interferes with our measurements. This is done simply by recording the acceptor excitation spectrum for a solution containing $(DA\text{-}coum)_2$-BPTI and $(MNA)_2$-BPTI at concentrations of 10^{-5} and 10^{-4} M with an excess of the donor-labeled protein (5-fold relative to the acceptor-labeled protein). The excitation spectrum of the acceptor recorded in the above experiment was identical with that obtained for DA-coum-BPTI in the absence of MNA-BPTI. Hence, this experiment shows both that no dimers are formed by doubly labeled BPTI under the conditions reported in this investigation and that only intramolecular energy transfer is measured for the (1-*n*)BPTI derivatives.

Equipped with the two references, 0% and 97% transfer efficiencies (DA-coum-BPTI and MNA-DA-coum-Lys, respectively), one can approach the quantitative steady-state measurements of transfer efficiencies. This is achieved by recording the acceptor excitation spectra. In Figure 7 are shown the excitation spectra of (1-15)BPTI (B) and (1-41)-BPTI (A), along with the excitation spectra of the references, all recorded at an emission wavelength of 480 nm under identical conditions, though at different concentrations. Comparison of excitation spectrum of MNA-DA-coum-Lys (MD-Lys) with that of DA-coum-BPTI clearly shows the contribution of the excitation of the donor to the emission of the acceptor. The excitation bands at 285, 295, 323, and 338 nm are characteristic of MNA excitation or absorption spectra. All spectra were normalized to equal emission intensity when excited at 382 nm. At this wavelength, there is no absorption by the donor and, hence, the observed intensity is directly related to DA-coum concentration and, therefore, is a reliable quantity to be used for normalization of all spectra. Once normalized, one can measure the difference between the excitation spectrum of any doubly labeled derivative and the DA-coum-BPTI (zero transfer). The ratio of integrated area under this difference spectrum in the range of 285–338 nm to the integrated difference spectrum calculated by the same procedure for MD-Lys (multiplied by $^{100}/_{97}$) gives quantitatively the excitation energy-transfer efficiency.

The same clear differences in transfer efficiencies between (1–41)BPTI and (1–15)BPTI found in the emission spectra appear in the excitation spectra. In (1–41)BPTI (Figure 7), a more efficient excitation energy transfer takes place (higher intensity of acceptor emission is obtained upon excitation in the donor absorption bands); this is interpreted as a shorter average interchromophoric distance. The concomitant decrease of donor emission and increase of acceptor emission in (1-41)BPTI relative to (1-15)BPTI indicates that the changes in the donor emission and acceptor excitation spectra are due to differences in intramolecular excitation energy-transfer

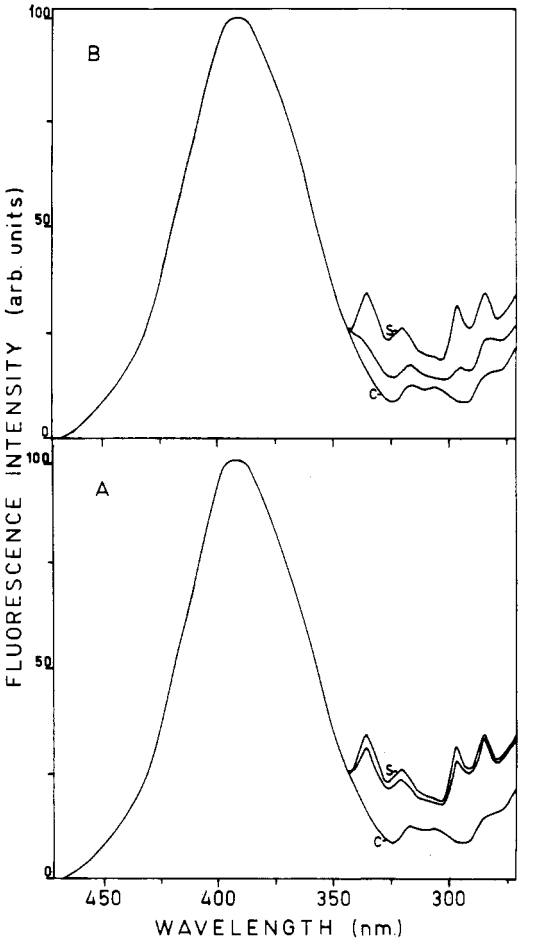

FIGURE 7: Acceptor fluorescence excitation spectra (uncorrected) (emission wavelength 480 nm) of BPTI derivatives and reference derivatives of 97% and 0% excitation transfer. The spectrum marked C is that of N^{ϵ}-DA-coum-Lys^{41}-BPTI, a derivative without donor and hence with 0% transfer. The spectrum marked S is that of MNA-DA-coum-Lys, a reference compound with 97% transfer efficiency. The unmarked traces are those recorded for (1-41)BPTI in (A) and (1-15)BPTI in (B) under identical conditions. All spectra were recorded at room temperature and normalized to constant intensity at 382 nm, where no absorption by the donor takes place. The derivatives (concentrations less than 2×10^{-6} M) were dissolved in 0.05 M bicine buffer, pH 7.5, with 0.1 M NaOAc. Excitation bandwidth 2 nm, emission bandwidth 12 nm. The excitation bands at 285, 295, 323, and 338 nm are characteristic for MNA, the donor. These spectra give a direct demonstration of the acceptor fluorescence contributed by donor absorption and excitation energy transfer.

efficiencies. Figure 8 shows the excitation spectra of (1-46)BPTI (A) and (1-26)BPTI (B) in the native state in aqueous neutral buffer. On the basis of the above considerations, the experimentally recorded excitation spectra were analyzed and transfer efficiencies were calculated for each derivative. The results are summarized in Table II.

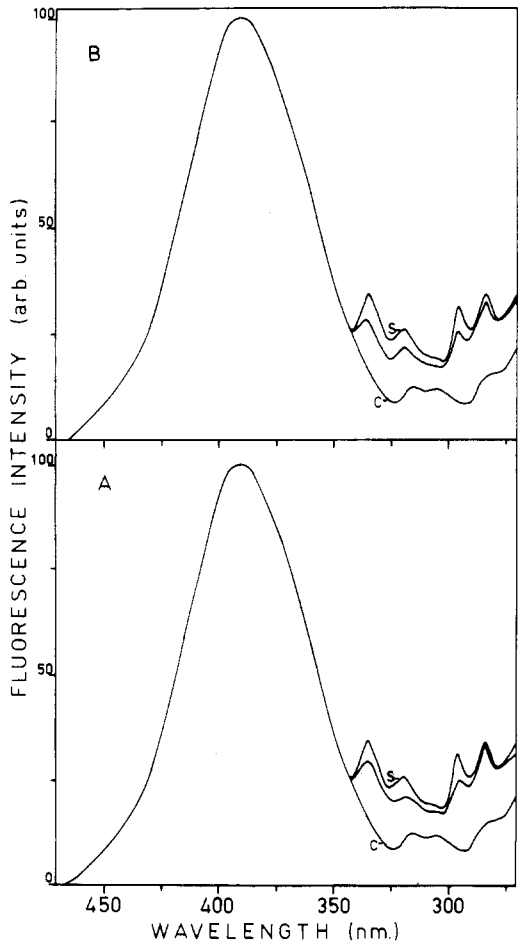

FIGURE 8: Acceptor excitation spectra of (1-26)BPTI (A) and (1-46)BPTI (B). Same conditions and designations as in Figure 7.

Intramolecular distances determined from steady-state measurements are average distances. These are equal to the root mean squared distances *only* when all molecules have exactly the same distance. A more quantitative analysis of excitation energy transfer in flexible molecules can be achieved by analyzing donor fluorescence decay kinetics and the deconvolution procedure described above.

Analysis of Donor Fluorescence Decay Curves. The fluorescence decay of MNA in MNA-BPTI and the derivatives (1-*n*)BPTI (n = 15, 26, 41, 46) was measured in aqueous buffer at neutral pH at room temperature and in 50% glycerol mixture with 0.1 M bicine buffer, pH 7.5, at −30 °C. Figure 9 shows the experimental decay curve $F(t)$ of MNA-BPTI analyzed by assuming a monoexponential decay kinetics. The calculated fluorescence decay constant in the aqueous buffer at room temperature is 6.8 ± 0.1 ns, and the RMS of fit is 0.0035. In 50% glycerol at −30 °C, *a single decay component* (8.1 ± 0.15 ns) is obtained (Figure 9). A small systematic deviation between the calculated and experimental traces is observed (less than 2%). This deviation defines the limits of significance of the analysis of energy-transfer experiments. The fact that a single decay constant is found for the donor when it is bound to the protein enables a simple analysis of energy-transfer measurements using eq 3 and 4. In this analysis, any deviation from monoexponential decay is interpreted as a deviation from a single interchromophoric distance, i.e., a distribution of distances.

The kinetics of the decay of fluorescence of the donor, MNA, in the four doubly labeled BPTI derivatives is characterized by shorter average lifetimes. In Figure 10A is shown the result of an experiment in which the fluorescence decay of the donor in (1-15)BPTI was measured in aqueous neutral buffer at room temperature. Fitting the experimental curve to a monoexponential decay function yields an average lifetime of 3.7 ns with an RMS of fit of 0.0050. This higher deviation from monoexponential decay, as compared with the decay of the donor in the absence of an acceptor (MNA-BPTI), is a clear manifestation of a distribution of transfer efficiencies caused in part by distribution intramolecular distances. A similar analysis of the fluorescence decay of the donor in the other three derivatives gave shorter lifetimes (of the order of 1 ns) and higher RMS. The decay curves obtained for the four BPTI derivatives were further analyzed by assuming a

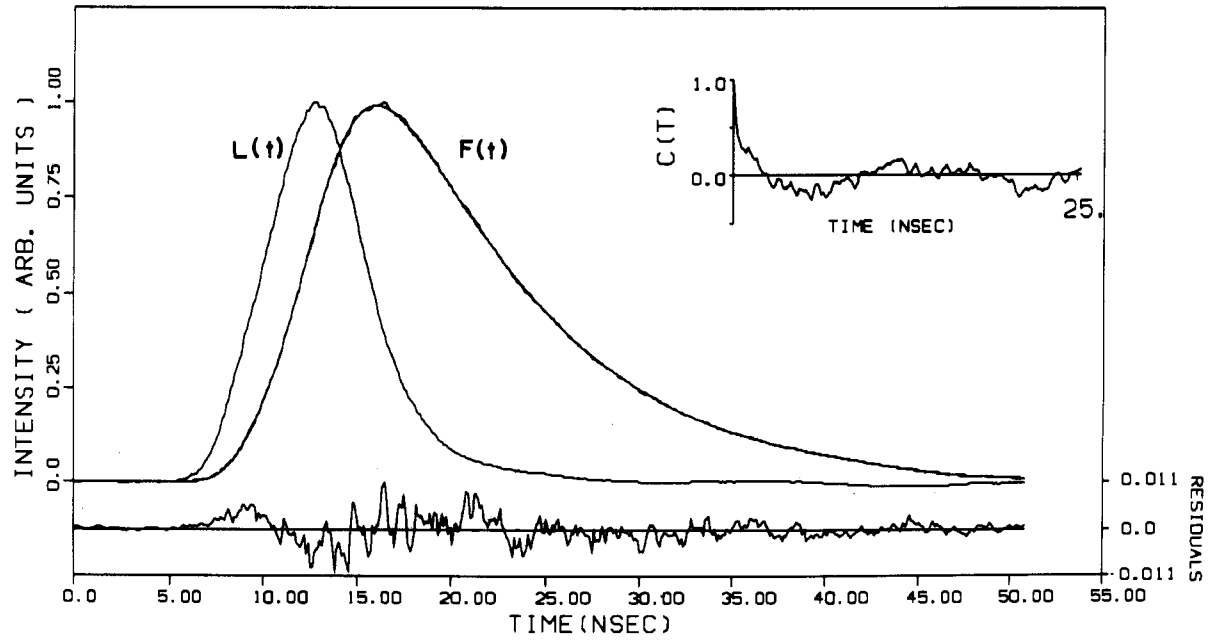

FIGURE 9: Fluorescence decay of the donor, MNA, in MNA-BPTI in 50% glycerol in 0.05 M bicine buffer, pH 7.5, at −30 °C. The experimental curve was fitted to a monoexponential decay function. The shortest pulse $L(t)$ is the trace of the excitation pulse. The second pulse, $F(t)$, shows the experimental and calculated donor fluorescence decay curves. The lower inset shows the deviation between the two curves, and the upper right inset shows the autocorrelation of the residuals. These show that the decay rate is monoexponential.

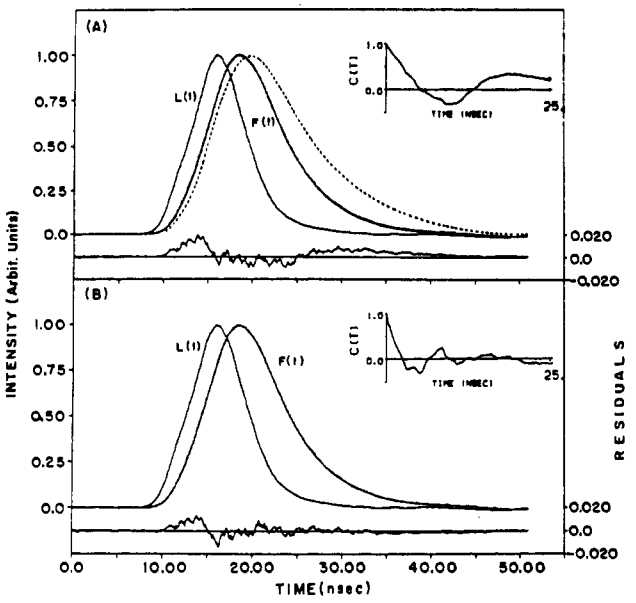

FIGURE 10: Fluorescence decay of the donor in (1-15)BPTI, in 0.05 M bicine buffer, pH 7.5, at room temperature. (A) Analysis assuming monoexponential decay. The distribution of the residuals and their autocorrelation function show a small deviation from monoexponential decay (RMS = 0.0050). (B) The same decay curve shown in (A) was reanalyzed by using eq 3. The best fit obtained with the parameters $a = 0.043$ and $b = 30.5$ is improved in comparison to the monoexponential fit shown in (A). RMS of fit equals 0.0035. The corresponding distribution function is shown in Figure 11. (---) Trace of donor fluorescence decay in the absence of an acceptor ($\tau = 6.8$ ns).

biexponential decay kinetics. An improved fit was obtained with low RMS of deviations. The weighted average lifetime

$$\tau_{av} = \sum_{i=1}^{n} \alpha_i \tau_i$$

where α_i are the normalized preexponentials, gives a direct measurement of E, the efficiency of excitation transfer, since $E = 1 - \tau_{av}/\tau$, where τ is the lifetime of the donor in the absence of an acceptor. The results are summarized in Table II and compared with the transfer efficiencies measured by the steady-state method. The two independent measurements are in reasonable agreement. The emission spectra are an important control for the interpretation of intensity changes in terms of excitation transfers. The steady-state measurement employs the acceptor emission; hence fractions of very high transfer efficiencies that may be missed in the donor fluorescence decay measurement (very short lifetimes) show up in this mode. Fractions with very low transfer efficiencies, which can be missed in the excitation spectrum (small contribution to acceptor emission), contribute long components to the donor fluorescence decay. Hence the combination of the two complementary modes of measurements and their agreements confirm the interpretation of the spectral changes in terms of changes in transfer efficiencies. It is pertinent to note that in both methods one analyzes the *shape of the curve* (excitation spectrum ratio of emission peaks or decay kinetics), which is an intrinsic property of the system, independent of concentration-related parameters or other inputs.

As obtained from the analysis of acceptor excitation spectra, (1-15)BPTI shows 45 ± 5% transfer efficiency in the native state. In (1-41)BPTI, (1-26)BPTI, and (1-46)BPTI the two labeled sites are much closer, yielding transfer efficiencies of 85 ± 5%, 79 ± 5%, and 78 ± 5% respectively.

The same decay curves were reanalyzed by fitting the experimental curves to a theoretical curve calculated by using

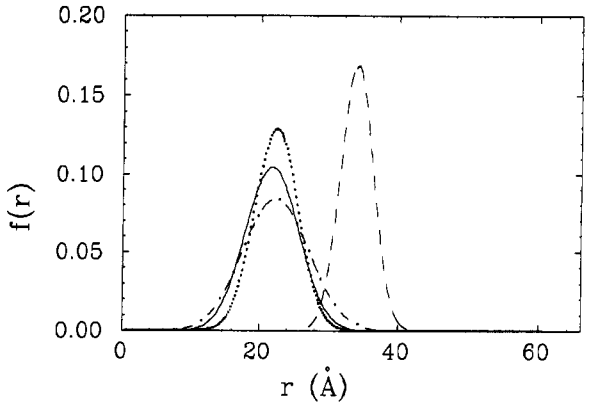

FIGURE 11: Intramolecular distance distributions in BPTI calculated from donor fluorescence decay curves obtained at room temperature (shown in Figure 10): (---) (1-15)BPTI, (···) (1-26)BPTI, (—) (1-41)BPTI, and (-·-) (1-46)BPTI.

eq 3 and 4. Figure 10B presents the same experimental fluorescence decay curve of (1-15)BPTI shown in Figure 10A, with the results of deconvolution analysis fitting it to a model of distance distribution. The RMS of fit is 0.0035, which is contributed mainly by the random noise, as can be judged by the randomness of the residuals and their low autocorrelation. The intramolecular distance distribution functions are presented in Figure 11. The average distance and the widths at half-height of all the distributions are included in Table II. Table II also gives the distances between the labeled amino groups as calculated from atomic coordinates derived from X-ray diffraction data (Wlodawer et al., 1984).

The striking feature emerging from the comparison given in Table II is that the *average distances* determined by our method *are very close to those expected from the known crystal structure of BPTI* when the extension by the probe and its attachment arm are taken into account. The *relative* differences between the distances between the four pairs of labeled sites are reproduced, the distance between residues 1 and 15 being by far the largest one.

The observed widths of the distributions are not entirely contributed by flexibility of the conformation of the protein. The distances obtained are related to the centers of the probes, which are connected to the labeled amino groups via a few bonds which may add up to 5 Å to the distances. The labeled ϵ-amino groups have some degree of flexibility which also contributes to the width of the distribution. Thus, the width of the observed interchromophoric distance distributions is clearly larger than the width of distribution of distances between the labeled amino groups at equilibrium (see Discussion).

The effect of dynamic fluctuations of the labeled segments is expected to increase the energy-transfer rate (Haas et al., 1978a) and therefore reduce the calculated average distances in the present analysis. In order to test whether our calculated distributions are shifted toward shorter distances by the fast conformational fluctuations, as has been observed for peptides and denatured protein (Haas et al., 1986), we have measured the fluorescence decay and excitation spectra of the labeled derivatives in highly viscous solutions. High viscosity is achieved by conducting the measurements in 50% glycerol (v/v) at −30 °C. Under these conditions, the viscosity of the solvent is larger than 70 cP (Miner & Dalton, 1953) and fast fluctuations are slowed down. The lifetime of MNA-BPTI in 50% glycerol in 0.05 M bicine buffer, pH 7.5 (the pH was measured at room temperature), increased to 8.1 ± 0.15 ns, and the monoexponential behavior of the decay kinetics is retained. The four doubly labeled derivatives (1-*n*)BPTI (*n*

= 15, 26, 41, 46) were measured under the same conditions. Excitation spectra recorded at −30 °C gave small changes in transfer efficiencies as compared to those obtained in the nonviscous aqueous buffer at room temperature. R_0 was calculated for the glycerol solution with the appropriate refractive index and Q (the emission and absorption spectra are not significantly changed) and found to be 32.2 Å. The results of analysis of the fluorescence decay of the doubly labeled BPTI derivatives in highly viscous solutions were very close to those obtained in buffer at room temperature. The main difference was a limited increase in the width of the distributions. This is well understood, since dynamic fluctuations are expected to reduce the apparent width, as compared to the equilibrium width.

Discussion

In this paper we have presented a method for studying the conformations of globular proteins that should be very useful in studying unordered or partially ordered conformational states either in equilibrium or as transients. The ability to measure intramolecular distance distributions and fast changes of conformations makes this method instrumental in the study of protein unfolding and refolding.

The key points essential for the applicability of the present approach are as follows: the preparation of a series of pure site specifically donor- and acceptor-labeled protein derivatives, minimalization of conformational interferences caused by the labels, a single R_0 for the whole ensemble of labeled molecules, and accurate fluorescence decay measurements free of any instrumental systematic deviation. These aspects will be discussed below.

The preparative procedures based on nonselective reactions, followed by high-resolution fractionations (Amir et al., 1985; Amir & Haas, 1986a), are relatively mild and have a minimal number of synthetic steps. MNA, the donor, does not change the net charge of the protein; thus the perturbation is further minimized. The labeled derivatives are as active as the unlabeled protein (except for the derivative blocked at its active site, Lys-15) and can, after reduction and denaturation, spontaneously refold, like the unlabeled protein, under the appropriate conditions. The kinetics of unfolding of the labeled derivatives, in 0.05 M bicine buffer containing 0.1 M sodium acetate, pH 8.0, and 0.01 M DTT at 26 °C, was monitored by loss of inhibitory activity, which measures the rate of loss of the overall structure of the molecule. Under these conditions, all the doubly labeled derivatives unfold at a rate that is about 3-fold faster than that of the native protein. This shows that for the doubly labeled derivatives the activation energy of the rate-determining conformational transition in unfolding is only 0.6 kcal lower than that for unlabeled BPTI. Thus, the presence of the covalently attached probes reduces the stability of one or more conformational intermediate(s), but no reduced activity is found. Furthermore, all three derivatives tested for rate of loss of activity in that experiment showed virtually the same kinetics. The site of labeling by the DA-coum does not affect the kinetics of unfolding when monitored by loss of inhibitory activity. BPTI is not unique in its relative insensitivity to blocking of amino groups. Other basic proteins were shown to be active even when many amino groups were blocked, e.g., histones (Jordano et al., 1985) and RNase (Frensdorf et al., 1967).

The monoexponential decay of the donor attached to the protein under all conditions measured allows for straightforward application of analysis based on eq 3 to the experimental data. In principle, the interchromophoric distance distribution function can be calculated even when the donor is not monoexponential, provided that the decay parameters τ_i and $\bar{\alpha}_i$ are well-known for all solution conditions employed. This condition adds further uncertainties in the experiments, and we prefer to avoid this by selecting for a donor characterized by a monoexponential decay. Thus, any deviation from monoexponential decay is a result of distance distribution, provided that R_0 and τ are constant for the whole ensemble of molecules. Furthermore, all competing deactivational processes are thus taken into account via τ, the donor fluorescence lifetime (eq 3), and variation of conditions does not prevent comparison of the resulting distributions. Monoexponential decay of a probe attached to a protein is not commonplace, and most naturally occurring probes are less useful for our studies due to nonexponential decay. Interestingly, in our system a monoexponential decay of MNA is found with or without a polarizer at the magic angle (35°) in the excitation beam.

The second parameter used in the analysis, R_0, was calculated from the spectral overlap integral, the refractive index of the medium, and the donor quantum yield (eq 1) following many studies that have shown the validity of the Förster theory (Latt et al., 1965; Stryer & Haugland, 1967; Gochanour & Fayer, 1981). Two points of uncertainty related to the Förster constant, R_0, should be discussed: first, its absolute magnitude and second, possible distortions of excitation-transfer rates by a distribution of R_0 values within the ensemble of molecules measured.

The comparison of the data obtained here on the basis of calculated R_0 values with known distances obtained from X-ray crystallography reassures that the calculated R_0 seems to be correct within the experimental uncertainties. Due to the size of the probe, one should expect the calculated average distance to be larger than those obtained by crystallography. Local conformations of the labeled sites may enhance the difference, as may be the case of (1-26)BPTI in which this difference is 5 Å. [In the preliminary report of this series of experiments (Amir & Haas, 1986b), a smaller R_0 was used (29.7 Å instead of 32.4 Å), and all distances reported were correspondingly erroneously smaller.]

The first source of uncertainty in the magnitude of R_0 is the dependence of transfer efficiency on the orientation of the probes. This may affect the analysis of distance distribution in two respects: (a) Unknown orientations lead to a wide range of possible κ^2 values, and thus a different scale (R_0) may be applicable for different derivatives. (b) A distribution of κ^2 values may lead to a distribution of transfer efficiencies even when a single distance is found. The extent of these uncertainties and means for narrowing their ranges have been discussed by many authors (Stryer, 1978; Jones, 1970; Dale et al., 1979; Hillel & Wu, 1976).

In an earlier paper (Haas et al., 1978b), we have shown that when the probes used have more than a single transition dipole of the emission, the extreme values of the orientation factor are eliminated and the distribution of possible κ^2 values is centered around the average of $^2/_3$. The problem turns into a matter of estimation of the possible error in the shape and average of the computed distance distributions due to the possible distributions of κ^2 values. When the probes rotate rapidly within the lifetime of the excited state, a single value of $\kappa^2 = {}^2/_3$ is justified. Fast rotation can be measured by the extent of fluorescence depolarizations; low values of $\langle r \rangle$, the fluorescence anisotropy, are indications of the completeness of orientational averaging during the lifetime of the excited state. A low value of the limiting anisotropy, r_0, is a result of mixed polarizations due to the participation of two or even

Table III: Average Fluorescence Anisotropies, $\langle r \rangle$, of Donor and Acceptor[a]

	MNA[b]		DA-coumarin[c]		
derivative	glycerol	H_2O	glycerol	H_2O	τ_{av} (ns)[d]
1-15	0.21	0.08	0.24	0.06	3.7 ● 0.2
1-26	0.20	0.09	0.25	0.06	1.1 ± 0.15
1-41	0.21	0.08	0.25	0.07	1.1 ± 0.15
1-46	0.20	0.06	0.24	0.05	1.2 ± 0.2
MNA-BPTI	0.19	0.03			6.8 ± 0.2
DA-coum-BPTI			0.24	0.06	
MD-Lys			0.22	0.013	

[a] Measurements were carried out at room temperature in either 0.05 M bicine buffer, pH 7.5 (H_2O), or 100% pure glycerol. [b] Donor fluorescence excited at 333 nm (2-nm bandwidth) and emission monitored at 360 nm (4-nm bandwidth). [c] Acceptor fluorescence excited at 380 nm (2-nm bandwidth) and emission monitored at 485 nm (10-nm bandwidth). [d] Average fluorescence lifetime of the donor, $\tau_{av} = \sum_i \alpha_i \tau_i$.

three orthogonal components in the relevant electronic transition (Albrecht, 1960). This is the case for symmetric aromatic chromophores as has been pointed out by Feofilov (1961). We have shown (Haas et al., 1978b) that measurements of limiting polarizations of the probes gives a quantitative estimation of the possible error in R_0, i.e., the width of the distribution of R_0 values assuming random orientation of the probe. Both MNA and DA-coum have medium limiting anisotropies, $r_0 \simeq 0.20$ and 0.23, respectively. Using our tables (Haas et al., 1978b), without taking into account the rotational relaxations, we find for this case that the width at half-height of the possible distribution of R_0 values is smaller than from 0.91 to 1.12, i.e., ±10%, and the extreme values possible for R_0 are 0.8 and 1.5 that of the averaged R_0.

Dale et al. (1979) have calculated the possible error in R_0 using a model of a single transition dipole. Using the anisotropy values measured for our probes (Table III) and Dale's graphs, one obtains a narrower range of extreme values. We have also measured the anisotropy of the fluorescence of the doubly labeled derivatives using 333-nm excitation and 485-nm emission wavelengths. This measurement gives an approximate value for the transfer depolarization (d_T in Dale's paper), but due to the subtraction of direct acceptor excitation, the uncertainty in these results is larger. For all the derivatives r_T thus obtained is between 0.01 and 0.05, giving a d_T^x value of 0.0–0.2. Hence, using Dale's Figures 4–8 (Dale et al., 1979), one obtains expected extreme values for κ^2 of 0.45 (minimum) and between 1.3 and 1.4 at the maximal end. This corresponds to a factor of 1.2 in R_0 or ±10% and represents the uncertainty arising from the unknown and incompletely averaged orientation of the probes. Both models are not strictly appropriate for the present experiment. The probes are attached to the globular protein, and therefore one cannot assume that all orientations of each probe are equally weighted, as assumed in our earlier analysis. Thus, we conclude that the correct value of R_0 for each one of our derivatives falls within the extreme values reported in our tables, but the shape of the distribution can be different due to the restrictions on the probes' orientation caused by the protein. The major issue in the context of the present experiment is that, due to possible specific local restrictions of configurations of the probes at each one of the four lysines, we may end up with different distributions of R_0 values and a different mean R_0 for each derivative. Both Dale's and our criteria cannot be straightforwardly applied here; the real mean value is somewhere in between. However, a few observations are relevant to this question: (a) All the derivatives share the same site of attachment of the donor. (b) The acceptor was attached to lysine side chains. Inspection of a model of BPTI crystal structure shows that lysines-15 and -26 are located at a longitudinal edge of the molecule and point out into the solvent. Lysine-46 is also placed in a position leaving a large degree of flexibility at the edge of the helical segment, while lysine-41 could be more restricted. (c) The rotational correlation time of the whole molecule, as deduced from Kasprzak's measurements of tyrosine depolarization (Kasprzak & Weber, 1982), is at least 13 ns. The rotational correlation times calculated for both probes using the Perrin equation are an order of magnitude lower. Thus, all the probes are freely rotating relative to the protein framework. The data presented in Tables II and III show that even though the average donor lifetime varies from 6.8 to 1.0 ns, its rotational correlation time is kept within less than a factor of 2 for all derivatives. The rotational correlation times obtained for the acceptor appear to be very short and independent of the site of labeling. This observation rules out possible local specific binding of the acceptor at the site of labeling and further reduces the uncertainty with regard to the correct R_0 value for each derivative. (d) We have measured the donor fluorescence decay of each derivative when dissolved in 50% glycerol in 0.05 M bicine buffer, pH 7.5. Measurements were carried out at room temperature and at −32 °C, thus changing solvent viscosity from 6 to >70 cP. In the low-temperature experiments, rotational freedom of the probes is restricted and we should expect the static-averaging regime to be dominant. If the dependence of R_0 on the orientation does follow the model of Dale et al., one should expect a significant shift in the distribution of transfer efficiencies or width of the distribution. However, the interprobe distance distribution functions calculated for all the derivatives in the frozen solution have virtually the same average and slightly larger width as compared to that observed at low viscosity (Amir & Haas, 1986b). (The increased width should be expected to result from an increased range of distances caused by the restricted dynamic averaging of probe and segmental configurations.) Thus, although we cannot quantitatively determine the narrow range of possible R_0 values, we have strong evidence that the uncertainty in R_0 is smaller than 10% that of the dynamically averaged value and that the use of a single value of R_0 for all derivatives is justified within less than a 10% error. Further narrowing of the range of uncertainty will be obtained by nanosecond fluorescence polarization experiments and introduction of another pair of probes to be used in our experiments (Stryer, 1978). These experiments are currently in progress in our laboratory.

Another source of uncertainty can arise from variations of the refractive index. A change of up to 10% in R_0 is possible between the two extreme values, 1.33 for the water and 1.5 for proteins. Based on the considerations presented by Moong et al. (1982), we tend to assume that contribution of the refractive index to variations of R_0 is less significant than other contributions.

Even two chromophores at a fixed single distance (e.g., if attached to a rigid molecule) will show an apparent distribution width due to the contribution of instrumental factors, which include nonlinearity of the detection system, background emission from the solvent including Raman scattering, and contaminations carried over with the purified protein samples.

The deviation from monoexponential decay and, hence, the calculated width of the distribution are very sensitive to minute amounts of contaminants. Even 3% of molecules with a donor without an acceptor cause significant skewness and increased width of the distribution. We have already improved our purification procedure to avoid contamination of the purified protein samples. An estimation of the contribution of these

factors to the width of the calculated distance distribution can be made on the basis of the noise level and the small deviation from monoexponential decay observed when the fluorescence decay of MNA-BPTI (donor only) is measured. A simple test, analysis of a decay curve of the donor in the absence of an acceptor using eq 3, gives an "apparent distribution" averaged at 100 Å a width of 3 Å. Thus, the experimental noise may contribute about 3 Å to the width of the calculated distributions (Table II, Figure 11).

The size of the probes is of the order of 6–7 Å; the "arm" attaching it to the protein includes two single bonds with rotational freedom for each one of them. It is assumed that the distance between the centers of chromophores is measured. If fast rotations take place, then transfer probabilities corresponding to the shorter interchromophoric distances are measured. Any restriction on this averaging will be manifested in a distribution of distances, within the size of the chromophore and the cone formed by the "arm" connecting it to the protein. This is the major factor contributing to the width of the distributions shown in Figure 11.

The flexibility of the protein backbone and the side chains that carry the probes contribute to the measured width of the distribution in the same manner as the size and the flexibility of the probe. Temperature factors reported for the amino groups of BPTI (Wlodawer et al., 1984) in the crystalline state yield calculated amplitudes of 0.5–0.8 Å and above. It is reasonable to assume that these motions are enhanced in solution. Amplified by the "arm" of the probe, it also contributes to the measured width of the distributions.

The size of the probe and its rotational freedom limit the resolution of determination of the shape and width of the intramolecular distance distributions by the present method. Since the probes attached to various sites on the protein molecule share a similar degree of rotational freedom (Tables II and III), we can consider the distributions shown in Figure 11 as the upper limit of the distribution width. It combines all the sources of deviation from monoexponential decays discussed above, including the flexibility of the native conformation. An interchromophoric distance distribution with similar width was obtained for a different pair of probes attached to residues 1 and 49 in ribonuclease A in its native state (Haas et al., 1987; McWerther et al., 1986). We have shown in the case of ribonuclease that the width of the distance distribution in the native state is contributed mainly by the conformational flexibility of the probes. Any change of the calculated distribution width, e.g., by denaturation, in which the rotational freedom of the probe is not restricted, can be attributed to a conformational change of the protein. It is pertinent to note that the uncertainty in the determination of the average of each intramolecular distance distribution is considerably smaller than its width. This is achieved by the analysis of the donor fluorescence decay curve (eq 3), which properly weighs the contribution of each conformer.

The results presented in this paper show that the methods developed in our laboratory enabled us to determine distributions of interluminophore distances for labels attached to a globular protein with a reasonable resolution, which should make this method useful in monitoring conformational changes. In terms of temporal and spatial range of detection, this method is complementary to other spectroscopic methods, such as nuclear magnetic resonance. Provided that orientational effects will be limited, it should enable monitoring localized conformational transitions, and the series of labeled derivatives that were prepared and those under preparation should be useful in monitoring of local structures and their transitions. This capability is very useful in studying the mechanism of protein folding, its intermediates, and their sequence of formation along the folding pathway.

Acknowledgments

We are grateful to Profs. E. Katchalski-Katzir and I. Z. Steinberg for invaluable encouragement and discussions. We thank Prof. G. L. Haberland and Dr. E. Wischhöfer, of Farbenbriken Bayer AG, for the kind gift of Trasylol. We thank Dr. A. Tishbi for his kind help in packing HPLC columns, R. August for careful technical assistance, and Dr. D. Levy for his important contributions. We thank Dr. T. Jovin for careful reading of the manuscript.

Supplementary Material Available

Details of the preparation of (1-*n*)BPTI (*n* = 15, 26, 41, 46), (1-15)BPTI, and MNA-DA-coum-Lys and a figure showing the reverse-phase HPLC separation of two structural isomers of MNA-DA-coum-Lys (5 pages). Ordering information is given on any current masthead page.

Registry No. DA-coum-NHSIE, 96686-59-8; MNA-DA-coum-Lys, 107175-25-7; L-Lys, 56-87-1; 2-methoxy-1-naphthyl aldehyde, 5392-12-1.

References

Albrecht, A. C. (1960) *J. Chem. Phys. 33*, 156–169.
Amir, D., & Haas, E. (1986a) *Int. J. Pept. Protein Res. 27*, 7–17.
Amir, D., & Haas, E. (1986b) *Biopolymers 25*, 235–240.
Amir, D., Varshavski, L., & Haas, E. (1985) *Biopolymers 24*, 623–638.
Amir, D., Levi, D. P., Levin, Y., & Haas, E. (1986) *Biopolymers 25*, 1645–1658.
Berlman, I. B. (1971) in *Handbook of Fluorescence Spectra of Aromatic Molecules*, p 130, Academic, New York.
Bundy, H. F. (1962) *Anal. Biochem. 64*, 431–435.
Chen, R. F., & Bowman, R. L. (1965) *Science (Washington, D.C.) 147*, 729–732.
Creighton, T. E. (1978) *Prog. Biophys. Mol. Biol. 33*, 231–287.
Creighton, T. E. (1984a) *Proteins*, W. H. Freeman, San Francisco.
Creighton, T. E. (1984b) *J. Mol. Biol. 179*, 497–526.
Dale, R. E., Eisinger, J., & Blumberg, W. E. (1979) *Biophys. J. 26*, 161–194.
Deisenhofer, J., & Steigmann, X. (1975) *Acta Crystallogr., Sect. B: Struct. Crystallogr. Cryst. Chem. B31*, 238–250.
Edwards, C. F. (1965) *Proc. Phys. Soc., London 85*, 613–624.
Erlanger, B. F., Kokowsky, N., & Cohen, W. (1961) *Arch. Biochem. Biophys. 95*, 271–278.
Feofilov, P. P. (1961) *The Physical Basis of Polarized Emission* (translated from Russian), pp 130–137, Consultant Bureau, New York.
Förster, Th. (1948) *Ann. Phys. (Leipzig) 2*, 55–75.
Frensdorf, A., Wilchek, M., & Sela, M. (1967) *Eur. J. Biochem. 1*, 281–288.
Gekko, K., & Timasheff, S. N. (1981) *Biochemistry 20*, 4677–4686.
Gochanour, C. R., & Fayer, M. D. (1981) *J Phys. Chem. 85*, 1989–1994.
Grinvald, A., & Steinberg, I. Z. (1974) *Anal. Biochem. 59*, 583–598.
Haas, E., Wilchek, M., Katchalski-Katzir, E., & Steinberg, I. Z. (1975) *Proc. Natl. Acad. Sci. U.S.A. 72*, 1807–1811.
Haas, E., Katchalski-Katzir, E., & Steinberg, I. Z. (1978a) *Biopolymers 17*, 11–31.

Haas, E., Katchalski-Katzir, E., & Steinberg, I. Z. (1978b) *Biochemistry 17*, 5064–5070.
Haas, E., McWherther, C. M., & Scheraga, H. A. (1987) *Biopolymers* (submitted for publication).
Handley, L., Coburn, T., Garwin, E., & Stryer, L. (1967) *Rev. Sci. Instrum. 38*, 488–492.
Hazan, G. (1973) Ph.D. Thesis, The Feinberg Graduate School of The Weizmann Institute of Science.
Hazan, G., Grinvald, A., Maytal, M., & Steinberg, I. Z. (1974) *Rev. Sci. Instrum. 45*, 1602–1604.
Hillel, Z., & Wu, C. W. (1976) *Biochemistry 15*, 2105–2113.
Jones, R. E. (1970) Ph.D. Thesis, Stanford University.
Jordano, J., Barbero, J. L., Montero, F., & Palacian, E. (1985) *Mol. Biol. Rep. 10*, 147–151.
Kasprzak, A., & Weber, G. (1982) *Biochemistry 21*, 5924–5927.
Kassel, B. (1970) *Methods Enzymol. 19*, 431–435.
Kim, P. S., & Baldwin, R. L. (1982) *Annu. Rev. Biochem. 51*, 459–489.
Latt, S., Cheung, H. T., & Blout, E. R. (1965) *J. Am. Chem. Soc. 87*, 995–1003.
Marquardt, D. W. (1963) *J. Soc. Ind. Appl. Math. 11*, 431–441.
McWherther, C. M., Haas, E., Leed, A. R., & Scheraga, H. A. (1986) *Biochemistry 25*, 1952–1963.
Miner, C. S., & Dalton, N. N., Eds. (1953) *Glycerol*, ACS Monograph 117, p 283, Reinhold, New York.
Moong, R. S., Kuki, A., Fayer, M. D., & Boxer, S. G. (1984) *Biochemistry 23*, 1564–1571.
Rigbi, M. (1970) in *Proceedings of the International Research Conference on Proteinase Inhibitors* (Fritz, M., & Tschesche, H., Eds.) pp 74–87, de Gruyter, Berlin.
Steinberg, I. Z. (1971) *Annu. Rev. Biochem. 40*, 83–114.
Steinberg, I. Z. (1975) in *Concepts in Biochemical Fluorescence* (Chen, R. F., & Edelhoch, H., Eds.) Vol. I, p 79, Marcel Dekker, New York.
Stryer, L. (1978) *Annu. Rev. Biochem. 47*, 819–846.
Stryer, L., & Haugland, R. P. (1967) *Proc. Natl. Acad. Sci. U.S.A. 58*, 719–720.
Vincent, J. P., & Lazdunski, M. (1972) *Biochemistry 11*, 2967–2976.
Vincent, J. P., Schweitz, H., & Lazdunski, M. (1974) *Eur. J. Biochem. 42*, 505–510.
Warshel, A., & Russell, S. T. (1984) *Q. Rev. Biophys. 17*, 283–422.
Wlodawer, A., Walter, J., Huber, R., & Sjolin, L. (1984) *J. Mol. Biol. 180*, 301–329.

Myelin Basic Protein Binds Heme at a Specific Site near the Tryptophan Residue

Stephen J. Morris,*,‡ Diane Bradley,‡ Anthony T. Campagnoni,§ and Gerald L. Stoner‡

Laboratory of Experimental Neuropathology, National Institute of Neurological and Communicative Disorders and Stroke, National Institutes of Health, Bethesda, Maryland 20892, and Mental Retardation Research Center, University of California at Los Angeles Center for the Health Sciences, Los Angeles, California 90024

Received April 25, 1986; Revised Manuscript Received October 28, 1986

ABSTRACT: Fluorescence of the single tryptophan residue in myelin basic protein (MBP) was excited directly at 295 nm (red-edge excitation) or at 278 nm which allows, in addition, indirect excitation by resonance energy transfer (RET) from any nearby tyrosine residues. Both red-edge excitation and the RET pathway were collisionally quenched by I^- and acrylamide, but not by Cs^+ or Co^{2+}, implying that the fluorophore is in an exposed, positively charged environment. The quenching coefficients (K) for I^- are 12–15 M^{-1} at both excitation wavelengths while coefficients for acrylamide are 15 M^{-1} at 278-nm and 8 M^{-1} at 295-nm excitation. Chloroheme, cyanoheme, and protoporphyrin IX also quench both red-edge excitation and the RET pathway with apparent quenching coefficients which are (2–5) $\times 10^4$-fold higher. This suggests that the mechanism of quenching now includes static in addition to collisional processes and thus that heme has a relatively high affinity for MBP. Scatchard analysis of the quenching suggests that chloroheme binds to MBP at two sites with dissociation constants (K_d) of 1.6×10^{-8} and 2.0×10^{-7} M and stoichiometries of 0.04:1 and 0.16:1, respectively. The hydrophobic fluorescent probe 4,4′-bis[1-(phenylamino)-8-naphthalenesulfonate] [bis(ANS)] binds to MBP less avidly ($K_d = 10^{-7}$ M) and is rapidly displaced by chloroheme ($K_i = 2 \times 10^{-8}$ M). The affinities of bis(ANS) and heme for MBP, along with the fluorescent amino acid quenching data, demonstrate that a subfraction of MBP molecules contain considerable structural specificity, implying stable long-range interactions in the molecule. Resonance energy transfer involving Trp and Tyr suggests a separation of these fluorophores of 10–15 Å or less. The location of the binding site for heme and bis(ANS), both of which require positively charged, hydrophobic environments, should be within the same distance constraints from the sole Trp. The distance requirements are satisfied by the β-sheet model for MBP [Stoner, G. L. (1984) *J. Neurochem. 43*, 433–447] which places Tyr-14 approximately 5 Å from Trp-117 on an adjacent β-strand. The requirement for a hydrophobic site with cationic character would be met if the heme/ANS binding site were located on the predicted β-sheet face near these residues.

The spectral properties of the naturally fluorescent amino acids tryptophan and tyrosine are useful as probes for their immediate environment in the protein polypeptide chain and also as indicators of long-range order in the molecule. For example, the fluorescence emission peak of the fluorophore shifts to lower wavelengths and the quantum yield increases with increasing hydrophobicity of its environment. In addition, two fluorophores with sufficiently high quantum yields and

* Address correspondence to this author.
‡ National Institute of Neurological and Communicative Disorders and Stroke.
§ UCLA Center for the Health Sciences.

0006-2960/87/0426-2175$01.50/0